

TRANSIENT RESPONSE OF 2D FLEXIBLE FOUNDATIONS RESTING ON THE SURFACE OF A TRANSVERSE ISOTROPIC VISCOELASTIC LAYER

Adolph, M.

Dept. of Computational Mechanics, Faculty of Mechanical Engineering, State University at Campinas – Unicamp, Brazil.

Mesquita, E.

Dept. of Computational Mechanics, Faculty of Mechanical Engineering, State University at Campinas – Unicamp, Brazil.
euclides@fem.unicamp.br

Barros, P. L. A.

Dept. of Geotechnique and Transportation, Faculty of civil Engineering, State University at Campinas – Unicamp, Brazil.

Abstract.

In the present article, the transient, vertical response of a 2D flexible and massless foundation resting on the surface of a transverse isotropic viscoelastic layer is presented. The foundation dynamic response is modeled by a stress boundary value problem, namely an uniformly distributed traction load applied at the layer surface. Initially the stress boundary value problem is solved in the frequency domain by means of the Fourier integral transform. The stationary response is synthesized numerically for very high response frequencies. The transient response is obtained by applying the Fast Fourier Algorithm (FFT) to the previously synthesized frequency domain solutions. The good quality of the high frequency responses allow the accurate calculation of the transient response at very small time steps. These solutions are used to perform a series of parametric studies. The relation between the foundation response and the wave propagation and reflection phenomena at the layer bottom is analyzed. The effect of the layer anisotropy on the transient response is reported. The influence of the domain viscoelastic models and constitutive parameters on the transient response is also analyzed. The issue of viscoelastic models and response causality is addressed. This solution procedure may be applied to synthesize transient viscoelastic anisotropic auxiliary states, which may be incorporated in the Boundary Element Method to yield the dynamic analysis of bounded and unbounded continua.

Keywords. Transient Response, Foundations, Viscoelastic, Anisotropy, Green's Functions

1. Introduction

When modeling the dynamic response of foundations, the soil may be best represented by an unbounded domain. In infinite domains energy is carried away from the perturbation sources in form of non-reflected waves. This phenomenon is known as geometric or radiation damping (Richard et al, 1970). The mathematical expression for this damping mechanism was given by Sommerfeld (1949) and is also known as the Sommerfeld Radiation Condition (SRC). Special techniques are required to include the SRC into domain type methods like the Finite Element Method (FEM) or the Finite Difference Method (FDM). These techniques include de Dirichlet-to-Neumann mapping (Zavalla & Pavanello, 1999) and the so-called Infinite Elements (Mesquita et al, 2002). On the other hand the Boundary Element Method (BEM) can naturally account for the SRC provided an auxiliary state satisfying this condition is available (Beskos 1987, 1997, Dominguez, 1993).

The purpose of this article is twofold. A transient stress boundary value problem of anisotropic viscoelastodynamics is solved. This solution may, in a first approach, describe the dynamic of a very flexible and also massless foundation resting at the soil surface. The solution allows a series of parametric studies including the effect of the layer depth, the viscoelastic constitutive models and parameters as well as the soil degree of anisotropy. Three distinct viscoelastic models are investigated, namely, the constant hysteretic, the Kelvin-Voigt and a "ramp-like" model. The synthesized solution may also be regarded as a transient viscoelastic anisotropic auxiliary state, which can be incorporated in the Boundary Element methodology to approximate the solution of more general boundary value problems. It should be mentioned that up to the present time there is no general transient viscoelastic anisotropic solution available to the BE formulation.

2. Solution of the stress boundary value problem in the frequency domain

The constitutive equations for two-dimensional transverse isotropic viscoelastic continua are given by (Barros, P.L.A. & Mesquita, E., 1999):

$$\begin{Bmatrix} \sigma_{xx} \\ \sigma_{zz} \\ \sigma_{xz} \end{Bmatrix} = \begin{bmatrix} c_{11} & c_{13} & 0 \\ c_{13} & c_{33} & 0 \\ 0 & 0 & c_{44} \end{bmatrix} \begin{Bmatrix} \varepsilon_{xx} \\ \varepsilon_{zz} \\ 2\varepsilon_{xz} \end{Bmatrix} \quad (1)$$

It is usual to describe the continuum degree of anisotropy by defining two indices n_1 and n_3 which have unit values for the isotropic medium $n_1=n_3=1$ and are defined in equations (2) for the transverse isotropic domain:

$$n_1 = c_{33} / c_{11} \quad , \quad n_3 = (c_{11} - 2c_{44}) / c_{13} \quad (2)$$

For the plain strain case and in the absence of body forces, the equations governing the continua in the frequency domain (ω) may be expressed in terms of the cartesian displacement components $\{u\} = \{u_x, u_z\}^T$ as:

$$\begin{aligned} c_{11}u_{x,xx} + c_{44}u_{x,zz} + (c_{13} + c_{44})u_{z,xz} + \rho\omega^2u_x &= 0 \\ c_{44}u_{z,xx} + c_{33}u_{z,zz} + (c_{13} + c_{44})u_{x,xz} + \rho\omega^2u_z &= 0 \end{aligned} \quad (3)$$

In equation (3) ρ is the continuum density and ω is the circular frequency. The boundary conditions for the Stress Boundary Value Problem (SPBV) are given in equations (4) bellow and can also be depicted at figure 1:

$$\begin{aligned} t_z(x, z=0) &= \begin{cases} t_z; |x| \leq a \\ 0; |x| > a \end{cases} \\ t_x(x, z=0) &= 0 \\ u_x(x, z=H) = u_z(x, z=H) &= 0 \end{aligned} \quad (4)$$

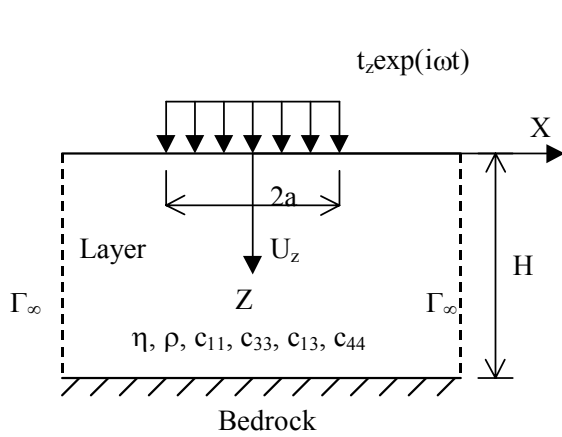


Figure 1. Massless and very soft foundation on a transverse isotropic viscoelastic layer

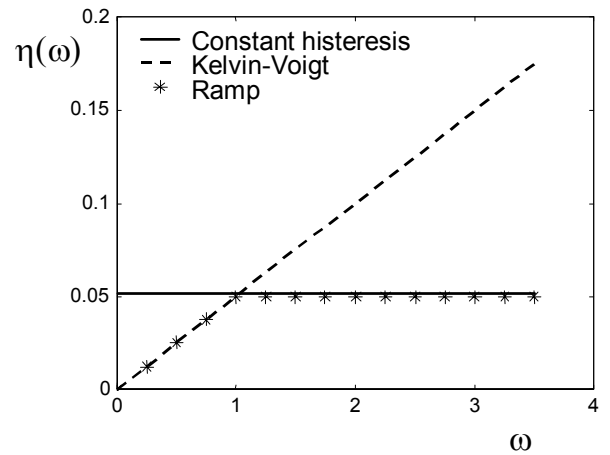


Figure 2. Frequency content of the damping factor $\eta(\omega)$ for distinct viscoelastic models

2.1 Viscoelastic models

Viscoelastic behavior is introduced through the elastic-viscoelastic correspondence principle (Christensen, 1982) by making the elastic constants complex:

$$c_{ij}^* = c_{1ij}^*(\omega) + i c_{2ij}^*(\omega) = c_{1ij}^*(\omega) [1 + i \eta_{ij}(\omega)] \quad , \quad (ij=11,33,13,44) \quad (5)$$

In equation (5) the indicated quantities define a storage modulus $c_{1ij}^*(\omega)$, a loss modulus $c_{2ij}^*(\omega)$ and a damping factor $\eta_{ij}(\omega) = c_{2ij}^*(\omega) / c_{1ij}^*(\omega)$. In this article the storage moduli are considered constant and possessing the value of the elastic counterpart, $c_{111}^*(\omega) = c_{11}$, $c_{133}^*(\omega) = c_{33}$, $c_{113}^*(\omega) = c_{13}$, $c_{144}^*(\omega) = c_{44}$. The damping factors are considered equal $\eta_{11}(\omega) = \eta_{33}(\omega) = \eta_{13}(\omega) = \eta_{44}(\omega) = \eta(\omega)$. Three distinct viscoelastic damping models are investigated, namely the constant hysteretic, the Kelvin-Voigt and a "ramp-like" model. The frequency content of the investigated damping factors is shown in Figure 2.

2.2 Frequency Domain Solutions

Defining a set of dimensionless parameters

$$\alpha = \frac{c_{33}}{c_{44}}, \quad \beta = \frac{c_{11}}{c_{44}}, \quad \kappa = \frac{c_{13} + c_{44}}{c_{44}}, \quad \delta^2 = \frac{\rho\omega^2}{c_{44}} \quad (6)$$

Equations (3) may be normalized to yield

$$\begin{aligned} \alpha u_{x,xx} + u_{x,zz} + \kappa u_{z,xz} + \delta^2 u_x &= 0 \\ u_{z,xx} + \alpha u_{z,zz} + \kappa u_{x,xz} + \delta^2 u_z &= 0 \end{aligned} \quad (7)$$

The Fourier integral transform with respect to the pair (x, λ) may be applied on equations (7) leading to:

$$\begin{aligned} -\beta^2 \lambda^2 \bar{u}_x + \bar{u}_{x,zz} + i\kappa \lambda \bar{u}_{z,x} + \delta^2 \bar{u}_x &= 0 \\ -\lambda^2 \bar{u}_z + \alpha \bar{u}_{z,zz} + i\kappa \lambda \bar{u}_{x,z} + \delta^2 \bar{u}_z &= 0 \end{aligned} \quad (8)$$

This set of coupled ordinary differential equations (8) may be uncoupled leading to two linearly dependent ordinary equations in the displacement variable u_x and u_z :

$$\begin{aligned} \beta \lambda^4 \bar{u}_x + \alpha \frac{\partial^4 \bar{u}_x}{\partial z^4} - \gamma \lambda^2 \frac{\partial^2 \bar{u}_x}{\partial z^2} - (1 + \beta) \lambda^2 \delta^2 \bar{u}_x + (1 + \alpha) \delta^2 \frac{\partial^2 \bar{u}_x}{\partial z^2} + \delta^4 \bar{u}_x &= 0 \\ \beta \lambda^4 \bar{u}_z + \alpha \frac{\partial^4 \bar{u}_z}{\partial z^4} - \gamma \lambda^2 \frac{\partial^2 \bar{u}_z}{\partial z^2} - (1 + \beta) \lambda^2 \delta^2 \bar{u}_z + (1 + \alpha) \delta^2 \frac{\partial^2 \bar{u}_z}{\partial z^2} + \delta^4 \bar{u}_z &= 0 \end{aligned} \quad (9)$$

The differential equations (9) possess a general solution in the form:

$$\begin{aligned} \bar{u}_x(\lambda, z) &= A_1 e^{-\delta \xi_1 z} + B_1 e^{\delta \xi_1 z} + A_2 e^{-\delta \xi_2 z} + B_2 e^{\delta \xi_2 z} \\ \bar{u}_z(\lambda, z) &= A_1' e^{-\delta \xi_1 z} + B_1' e^{\delta \xi_1 z} + A_2' e^{-\delta \xi_2 z} + B_2' e^{\delta \xi_2 z} \end{aligned} \quad (10)$$

The factors ξ_1 and ξ_2 in equation (10) are the eigen-values of the coupled operator shown in equations (8). The constants A_i, A_i', B_i and B_i' ($i=1,2$) present in (10) must be determined from the boundary conditions (4). Detailed expressions for these constants may be found in the work of Barros (Barros, P.L.A., 1997). Through a numerical inverse Fourier transformation of equations (10) with respect to the pair (λ, x) , the displacement solution in the original space-frequency domain (x, z, ω) may be determined:

$$\begin{aligned} u_x(x, z, \omega) &= \frac{\delta}{\sqrt{2\pi}} \int_{-\infty}^{\infty} \sum_{m=1}^2 \left(A_m' e^{-\delta \xi_m z} + B_m' e^{\delta \xi_m z} \right) e^{i\lambda x} d\lambda \\ u_z(x, z, \omega) &= \frac{\delta}{\sqrt{2\pi}} \int_{-\infty}^{\infty} \sum_{m=1}^2 \left(A_m e^{-\delta \xi_m z} + B_m e^{\delta \xi_m z} \right) e^{i\lambda x} d\lambda \end{aligned} \quad (11)$$

A numerical integration strategy has been developed to solve equations (11) and to yield accurate solutions at very high frequencies (Barros, P.L.A., 1997). Figures 3 show a typical displacement solution plotted for the dimensionless frequency $A_0 = \omega a / c_{44}$. The layer resonances in the vertical direction are clearly recognized in the solution. It should be stressed that from the physical point of view all significant phenomena take place at relative low frequencies $A_0 < 10$. The high frequency components are calculated to provide small time-steps for the transient response. The frequency solutions given in figures 3 were determined for an isotropic continua ($n_1 = n_3 = 1$), for a layer depth $H = 4a$ and for a constant hysteretic viscoelastic model with damping factor $\eta = 0.05$. Figures 3 also show that the dynamics of a layer over bedrock is quite involved. This intricate behavior will also be present in the transient response. Although only displacement solutions have been given, it is also possible to determine the components of the pertinent stress tensors.

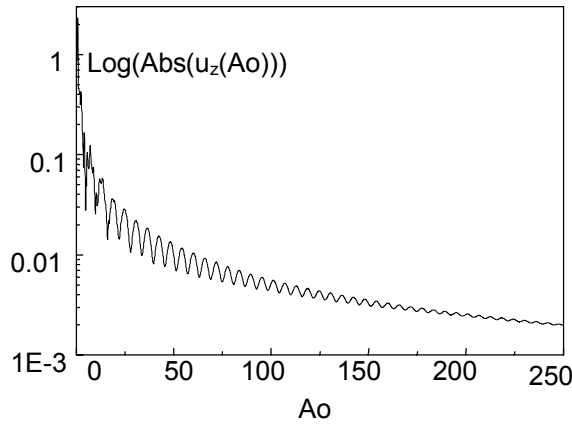


Figure 3a. Stationary displacement vertical solution u_z due to a vertical uniformly distributed surface load t_z

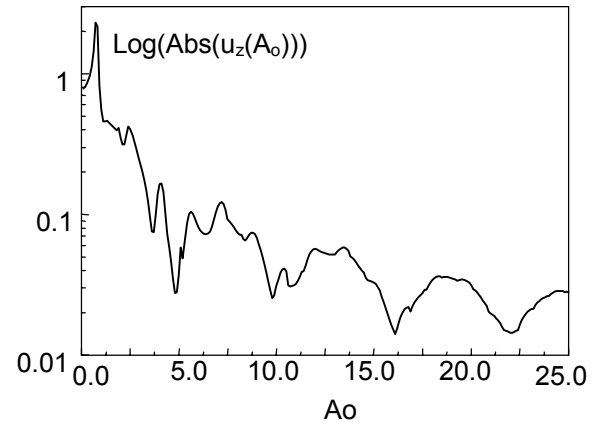


Figure 3b. Detail of the initial frequency steps

3. Transient Responses

The transient solution is obtained by applying the Fast Fourier Transform (FFT) algorithm with respect to the pair (ω, t) to the solutions given in equations (11). One important issue of the discrete FT is the relation between the frequency step $\Delta\omega = \omega_{k+1} - \omega_k$ and the maximum time reachable in the transient process, $T_{\max} = 2\pi/\Delta\omega$. Analogously, the relation between the time step Δt and the maximum sampling frequency ω_{\max} is: $\Delta t = 2\pi/\omega_{\max}$. So it is desirable to have frequency solutions at very small steps $\Delta\omega$ and also at very large maximum sampling frequencies ω_{\max} . However, it should be stressed that the determination of frequency domain solutions is computationally very expensive. So, in order to yield small steps and large final frequencies the domain solutions $u_i(\omega)$ must undergo a mathematical treatment. The same reasoning applies to the dimensionless frequency A_o .

Figure 4 shows, schematically, the mathematical manipulation that is applied to the frequency solutions. The functions $u_i(A_o)$ ($i=x, z$) are calculated numerically, with a frequency step ΔA_o in the range $0 < A_o < A_{o \text{ calc}}$. To obtain a smaller frequency step in this range, the function is interpolated with cubic splines. Beyond the frequency $A_{o \text{ calc}}$ the numerical integration scheme fails or it is extremely time consuming. Above the cut-off frequency $A_{o \text{ zero}}$ the functions are assumed to vanish, $u_i(A_o > A_{o \text{ zero}}) = 0$. In the range between $A_{o \text{ calc}} < A_o < A_{o \text{ zero}}$ the functions are also interpolated by cubic splines, leading to a smooth transition between the frequency points $A_{o \text{ calc}}$ and $A_{o \text{ zero}}$. For low damping values the stationary response presents high oscillations at $A_{o \text{ calc}}$. In this case splines do not lead to a smooth transition and an exponential filter can be applied (Adolph, 2002).

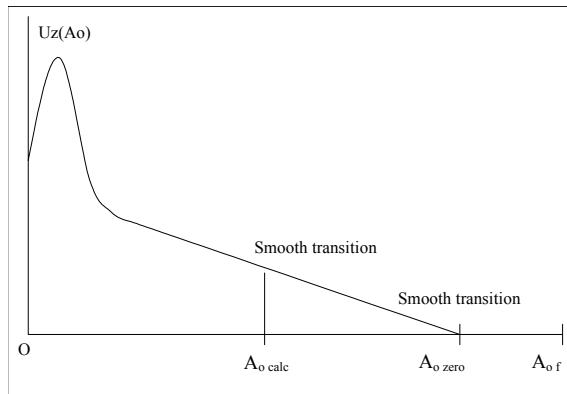


Figure 4: Scheme for treating the frequency solutions

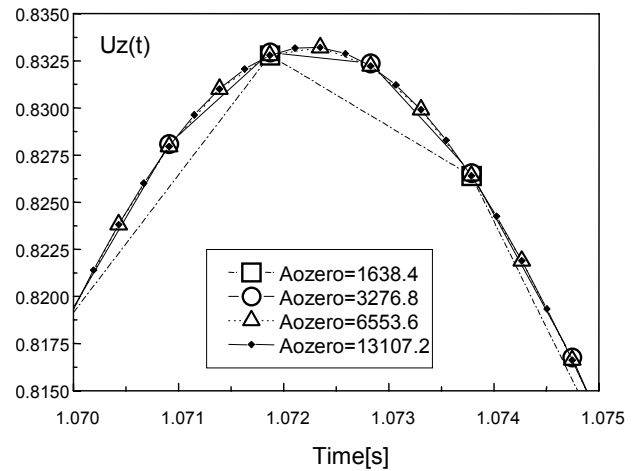


Figure 5: Effect of the including zeros between $A_{o \text{ zero}} < A_o < A_{o \text{ f}}$

Beyond the cut-off frequency $A_{o \text{ zero}}$ the solution is filled with zeros $u_i(A_{o \text{ zero}} < A_o < A_{o \text{ f}}) = 0$. If all significant information from the frequency signals has been determined in the range $0 < A_o < A_{o \text{ zero}}$, then filling the response with zeros should only lead to smaller time steps, without changing the transient response itself. This effect is shown in figure 5 for the solution $u_z(t)$ for a time instant at which the response reaches a peak. The constant hysteretic model with damping $\eta = 0.05$ was used and the considered layer depth was $H = 4a$. The solution is numerically calculated up to the frequency $A_{o \text{ calc}} = A_{o \text{ zero}} = 1000$. Between $A_{o \text{ zero}}$ and $A_{o \text{ f}}$ the solution is filled with zeros. Four distinct values of the maximum frequency were studied, $A_{o \text{ f}1} = 1638.4$, $A_{o \text{ f}2} = 3276.8$, $A_{o \text{ f}3} = 6553.6$, $A_{o \text{ f}4} = 13107.2$. The frequency step was

$\Delta A_o=0.0125$ leading to four distinct final number of discrete sampling points given, respectively, by: $k_1=131072$, $k_2=262144$, $k_3=262144$, $k_4=1048576$. An analysis of figure 5 shows, as expected, that adding zeros to the end of the response spectrum only leads to smaller time steps, without changing the transient response itself.

Next, the influence of the frequency step ΔA_o is addressed. The frequency response was calculated with three steps, namely $\Delta A_o=0.05$, $\Delta A_o=0.025$ and $\Delta A_o=0.0125$. Figures 6 shows the effect on the transient response. It can be seen that as ΔA_o decreases the maximum time T_{max} increases proportionally, as expected. No significant signal distortion is introduced by increasing the frequency step, as can be seen in figure 6b.

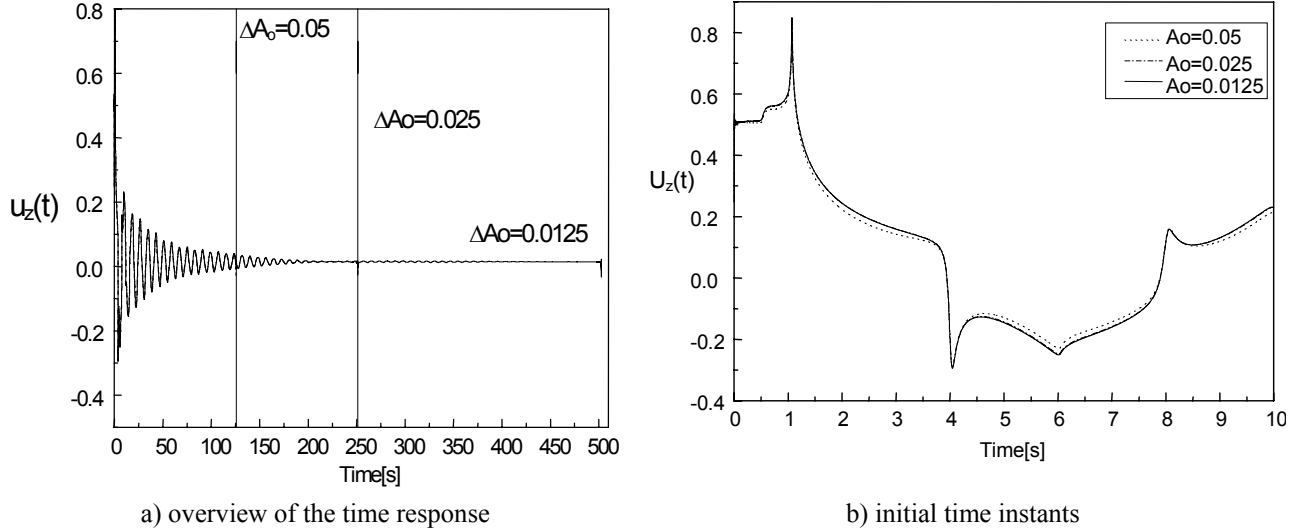


Figure 6. Influence of ΔA_o on the transient response.

4. Numerical results

In this section, numerically synthesized transient responses for the layer over the bedrock will be reported. The influence of the layer depth, viscoelastic model and parameters and the degree of anisotropy will be investigated. Initially, the transient response of a point situated at the layer surface at the center of the loading area ($x=z=0.0$) will be correlated to the wave propagation process taking place at the excited layer. Consider an isotropic viscoelastic layer ($n_1=n_3=1$) of depth $H=4a$, possessing hysteretic damping with coefficient $\eta=0.05$, density $\rho=1\text{kg/m}^3$ and elastic constitutive parameters $c_{44}=1\text{ N/m}^2$, $c_{11}=c_{33}=4\text{ N/m}^2$, $c_{13}=2\text{ N/m}^2$, subjected to the uniformly distributed spatial load, given in equation (4), and a Dirac's Delta impulse in time $f(t)=\delta(0)$. With these constitutive parameters the layer presents a dilatational wave velocity $p_1=2\text{ [a/s]}$, shear velocity $c_1=1\text{ [a/s]}$ and a Rayleigh wave velocity $c_R\approx 0.95\text{ [a/s]}$. In the range ($0.0 < A_o < A_{ocalc}$) the stationary responses were generated with a dimensionless frequency step $\Delta A_o=0.0125$. The other frequency parameters are $A_{ocalc}=A_{ozero}=1000$, $A_{of}=1638.4$. A total of 131072 frequency terms were used. The correspondent transient response has a period $T_{max}=502.65\text{ s}$ and a time step $\Delta t=0.019\text{ s}$.

Figure 7 furnishes the transient vertical displacement of the point ($x=z=0$) for the initial time instants. The response for larger times can be seen in figure 8. A sequence of snapshots showing the evolution of the layer vertical displacement component $u_z(x,z,t)$ at these initial time instants, that can be depicted in figures 9, explain the response obtained in figure 7. After a very abrupt initial response ($t=0+\Delta t$) the displacement remains almost stable at the value $u_z\approx 0.5$, until approximately $t\approx 0.55\text{ s}$ when there is a slight increase in the displacement, due to p-waves arriving from the corners of the spatial excitation. The displacement continues stable at this level until the sequence or train of s-waves and Rayleigh-waves generated at the corners of the spatial excitation arrive generating an amplitude peak at approximately $t\approx 1.1\text{ s}$. After this peak the displacement amplitude decreases monotonically until the first reflected wave appears, as will be described in the sequence.

To analyze the transient behavior at larger time steps, the wave reflections at the rigid base must be considered. Figure 8 shows the transient response at the origin ($x=z=0$) of a layer over bedrock with depth $H=2a$ for a larger response time. The same figure 8 also shows the transient response of a half-space in which no waves are reflected back to the surface. In order to interpret the results presented in figure 8, a scheme containing some possible trajectories from waves emanating from the surface and reflected at the rigid base is given in figure 10. The idea is to indicate that as the spatial excitation distribution is continuous, the reflected waves will also arrive continuously at the measuring point ($x=z=0$), breaking the original sharp wave fronts.

Figures 11 show, schematically, the pattern of wave propagation and reflection at various time instants for a layer with depth $H=2a$. It is known that at the initial time instants p-waves (dilatational) and s-waves (shear) are sent towards the rigid base with velocities $p_1=2\text{ a/s}$ and $c_1=1\text{ a/s}$, respectively. Surface Rayleigh waves are kept close to the surface and will not be included in propagation pattern. At time $t=1\text{ s}$ the p_1 wave reaches the rigid base $H=2a$ and is reflected back as a p_{p1} wave and as a shear wave c_{p1} . At time $t=2\text{ s}$ the p_{p1} wave reaches back the layer surface. At this instant the c_1 wave reaches the bottom and is reflected as a dilatational p_{c1} and a c_{c1} shear wave. The influence of p_{p1} reaching back

the surface as a traction wave can readily be recognized in figure 8. The propagation pattern may be followed in figure 11. The arrival of c_{p1} and p_{c1} at $t=3s$ is clear at the picture. At $t=4s$ the p_{ppp1} and c_{c1} reaches the surface, and so on. In the context of the present article it is important to recognize that all these features are present in the numerically determined transient solution.

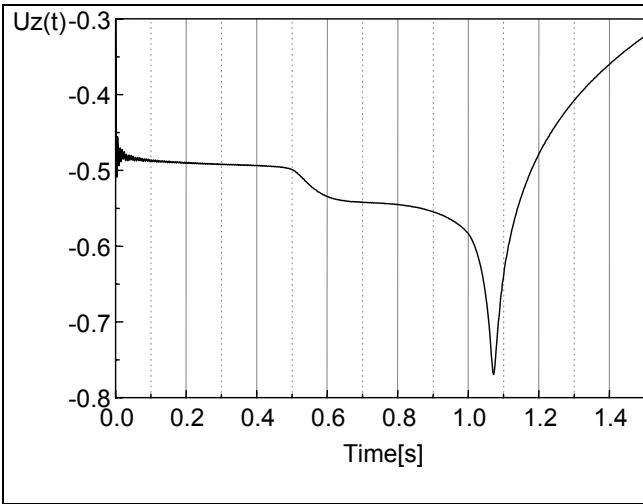


Figure 7: Initial time steps of the transient layer response

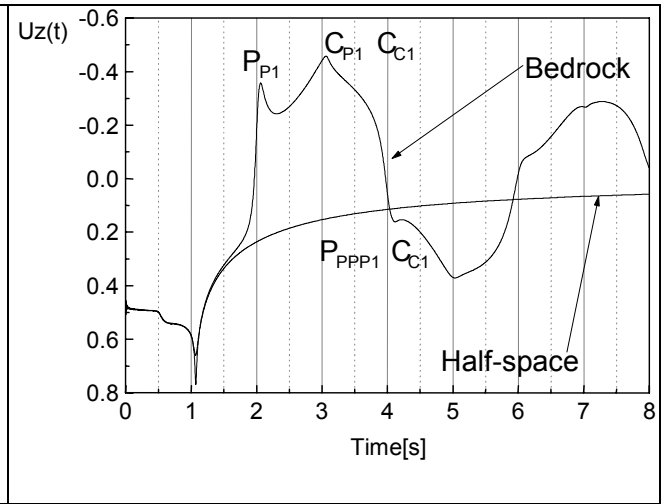
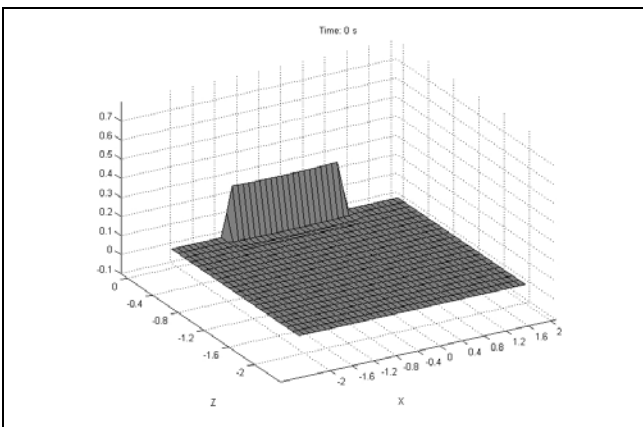
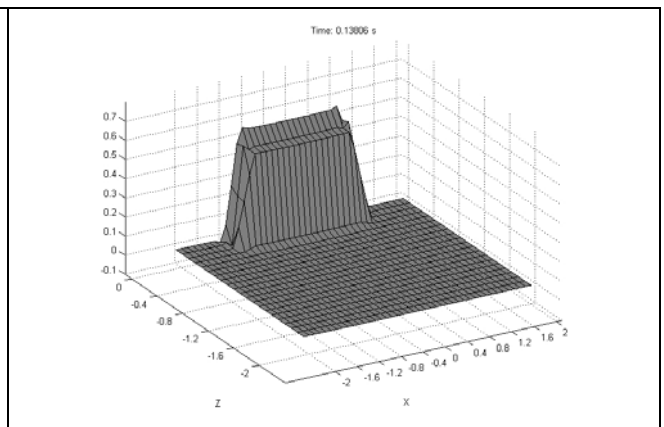


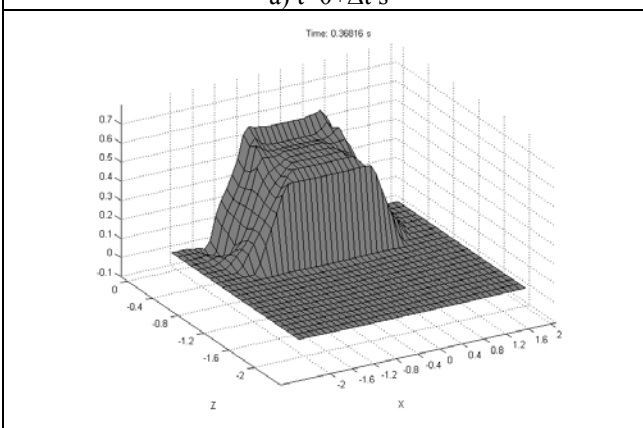
Figure 8: Layer transient response for larger response instants



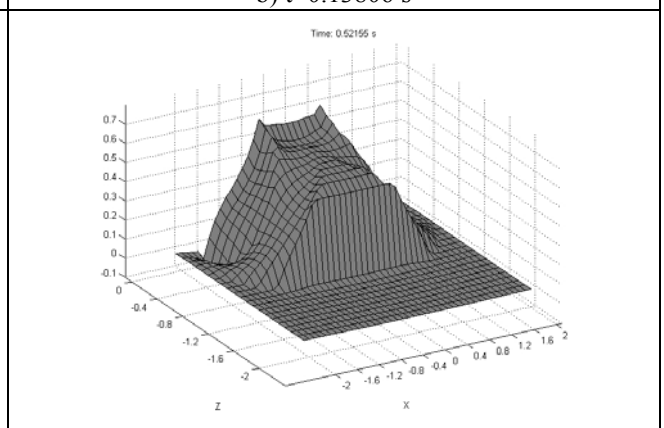
a) $t=0+\Delta t$ s



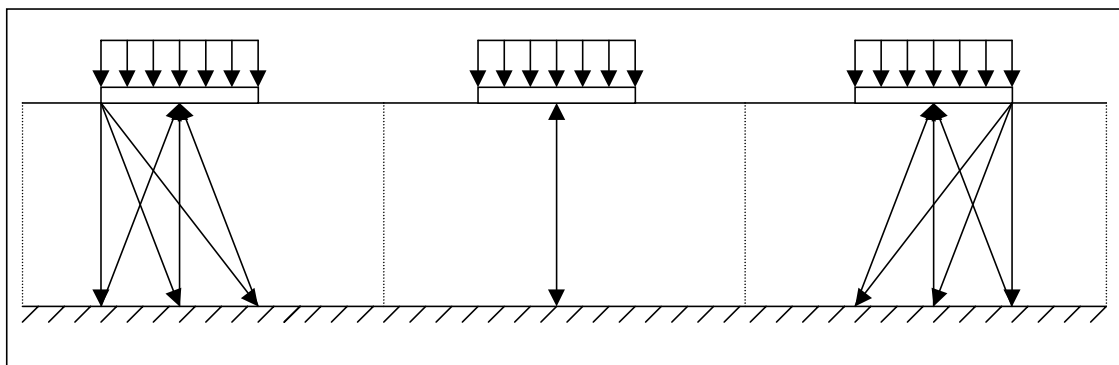
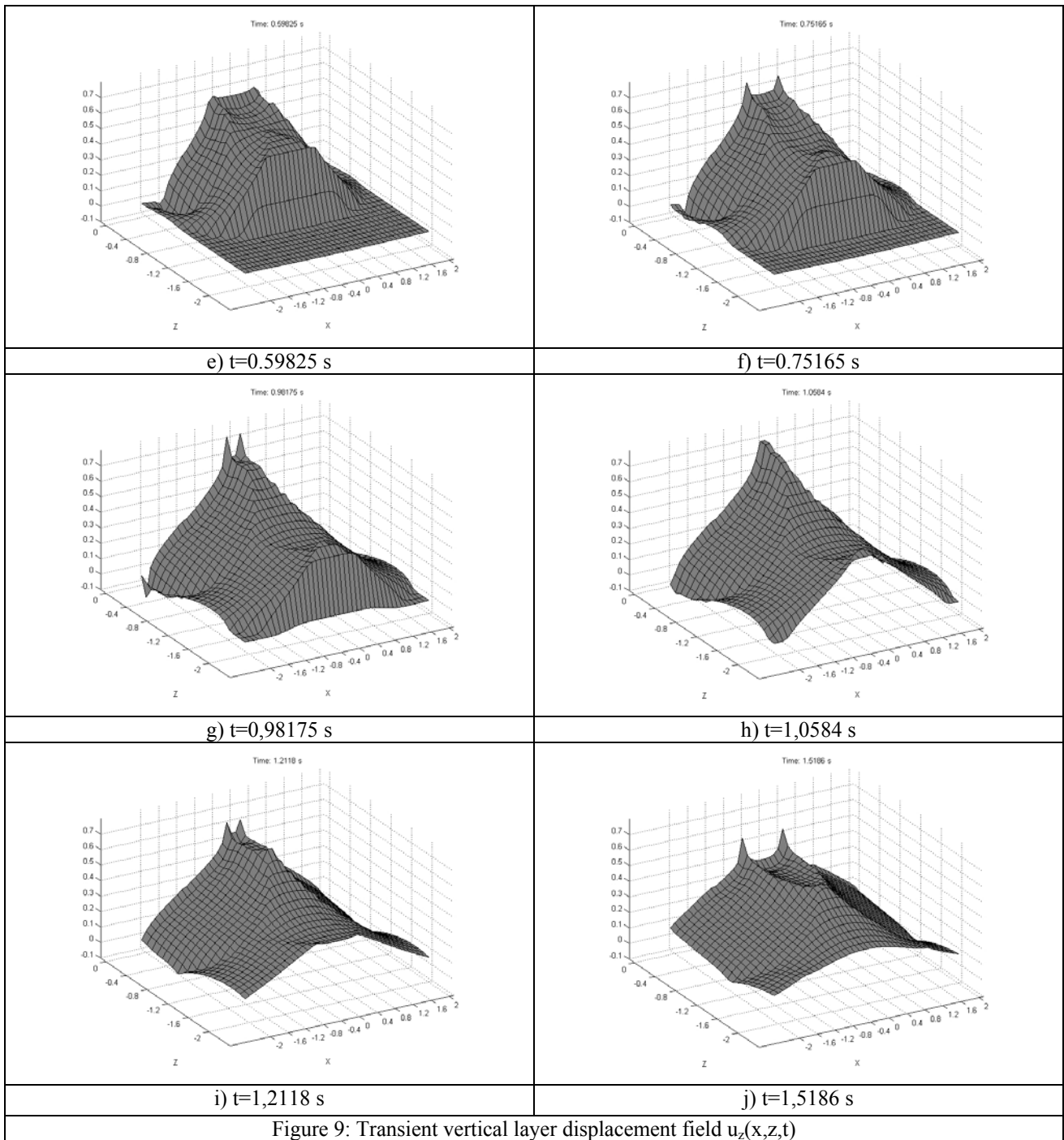
b) $t=0.13806$ s



c) $t=0.36816$ s



d) $t=0.52155$ s



4.1 Influence of the viscoelastic model on the transient response. In the sequence the effect of the viscoelastic models and damping parameters on the transient response is investigated. Consider an isotropic viscoelastic layer with

$H=4A$. and the same material properties of the example shown in figure 7, subjected to a Dirac's Delta time excitation $f(t)=\delta(t=0)$. Three damping models, namely, the constant hysteretic, Kelvin-Voigt and "ramp-like" model with damping coefficients $\eta=0.05, 0.1, 0.2$ are investigated. Figure 12 shows the influence of the damping parameter for the constant hysteretic model. As expected, increasing the damping will lead to smaller displacement amplitudes. The same response for a Kelvin-Voigt model is depicted in figure 13.

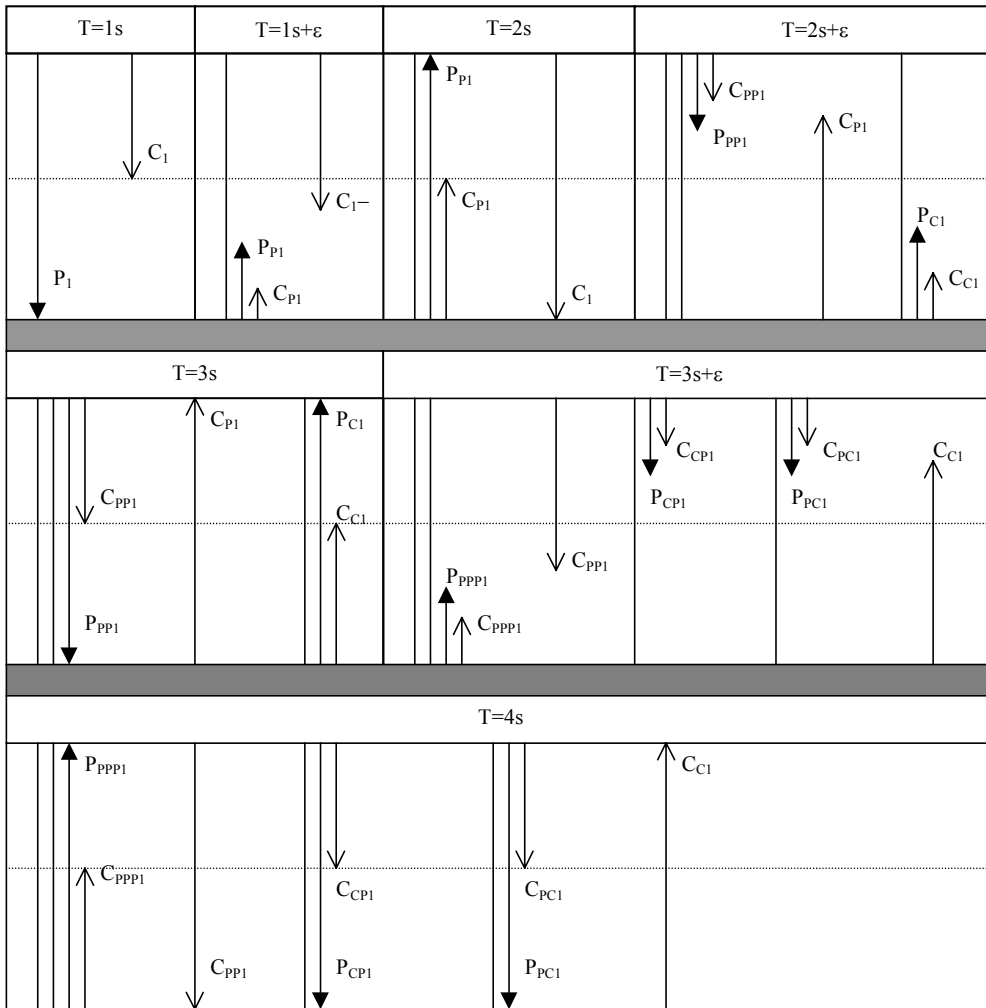


Figure 11: Scheme of wave propagation with reflection at the rigid base

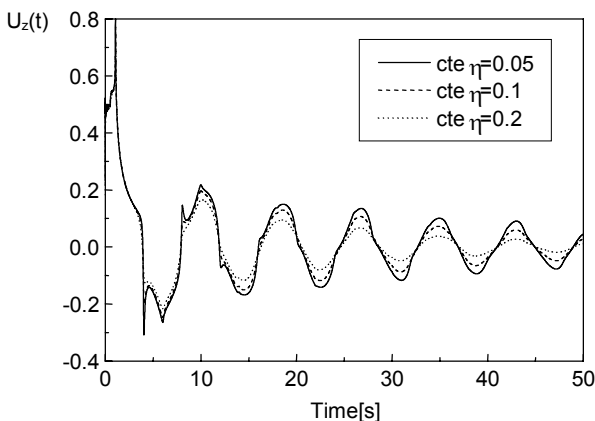


Figure 12: Displacement $u_z(t)$ for distinct values of the damping coefficient η - constant hysteretic model

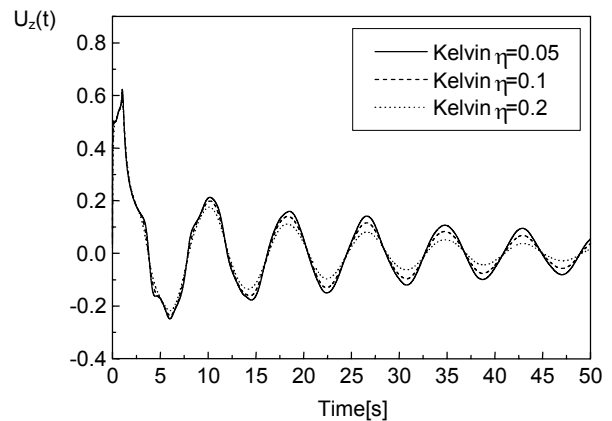


Figure 13: Displacement $u_z(t)$ for distinct values of the damping coefficient η - Kelvin-Voigt model

Figure 14 shows a comparison of the initial time response for three damping models possessing the damping coefficient $\eta=0.05$. The Kelvin-Voigt model gives a smaller response peak, but also in a smoother response. This is a consistent result. The large Kelvin-Voigt damping coefficients at high frequencies damp out the high frequency components in the stationary response, which are responsible for the abrupt changes in the transient solution.

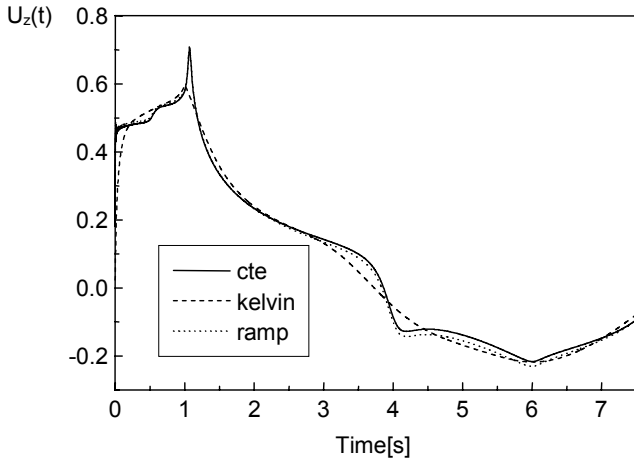


Figure 14: Comparison of distinct viscoelastic models – initial time steps, $\eta=0.1$

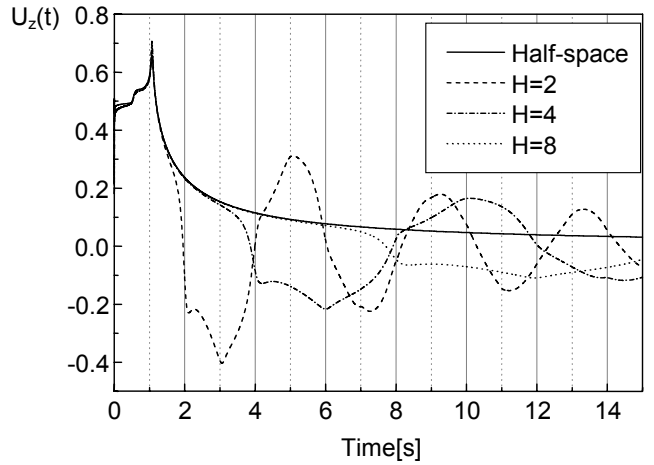


Figure 15: Effect of the layer depth on the transient response

4.2 Influence of the layer depth. As can be seen in figure 15, the layer depth causes two distinct effects on the transient response. For deeper layers the path that must be traveled by the waves prior to the arrival back at the surface increases. The consequences are that the reflected waves impinge the surface at later times with smaller amplitudes, due larger energy dissipation (geometric and internal). All these phenomena are well characterized in the response shown in figure 15. The example considered a hysteretic damping with $\eta=0.1$. Other properties are those of the previous examples.

4.3 Influence of the layer degree of anisotropy. The transient response of a transverse isotropic layer with depth $H=8A$ is given in figure 16. The constant hysteretic model with damping $\eta=0.05$ is considered. The material properties for the isotropic layer are: $\rho=1\text{kg/m}^3$, $c_{44}=1\text{ N/m}^2$, $c_{11}=c_{33}=4\text{ N/m}^2$, $c_{13}=2\text{ N/m}^2$. Two distinct cases are investigated. In the first case the anisotropy indices defined in equation (2) are set to $n_1=2.0$, $n_3=0.5$. The basic effect of this setting is that the vertical stiffness, in the z -direction, is increased leading to a faster dilatational wave front and smaller wave travel times downward. The second choice of anisotropy indices is $n_1=0.5$, $n_3=2.0$. This causes a lower vertical stiffness, compared to the isotropic case and, consequently, smaller wave speeds with larger travel times. It should also be noted that for softer layers the response amplitude tends to increase significantly. All these features may be found in the response shown in figure 16.

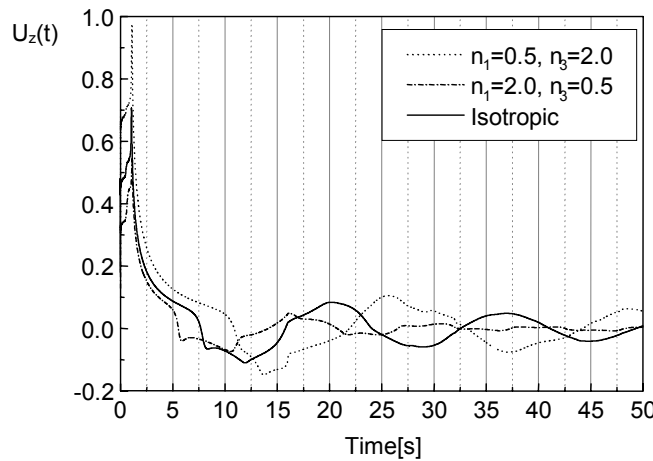


Figure 16: Response of transverse isotropic layer: influence of anisotropy degree

Analysis of Causality. It is well known that the FFT algorithm furnishes periodic responses. So the response for the largest time T_{\max} is connected to the initial time $T=0$. This means that the response at T_{\max} gives information about the causality of the obtained transient solution. Figures 17 and 18 gives the influence of the damping model on the causal behavior of a typical layer. The last time steps of the response are depicted. It should be noted that a causal behavior would present a vanishing solution at the last steps.

Figure 17 shows the effect of the damping ratio η for the constant hysteretic model. It is well known that this is a non-causal viscoelastic model. In this model the static or quasi-static solution ($A_0 \rightarrow 0$) presents a non-vanishing complex part related to the material damping. In figure 17, as the damping decreases and the solution tends to the causal

elastic case, the transient solution becomes increasingly causal. Figure 18 show the effect of the damping model on the response causality for a damping ratio $\eta=0.1$. It can be noticed that the Kelvin-Voigt model leads to a more causal response than the other analyzed models. Only at the very last time steps the K-V model shows some non-causal behavior. The results reported indicated that the present methodology may be used to assess the relation between damping models and causality.

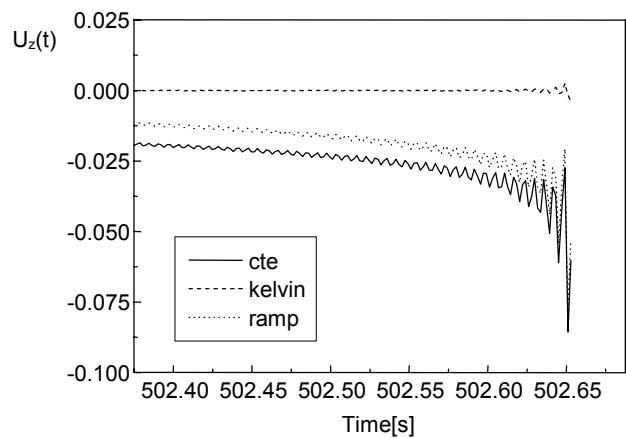
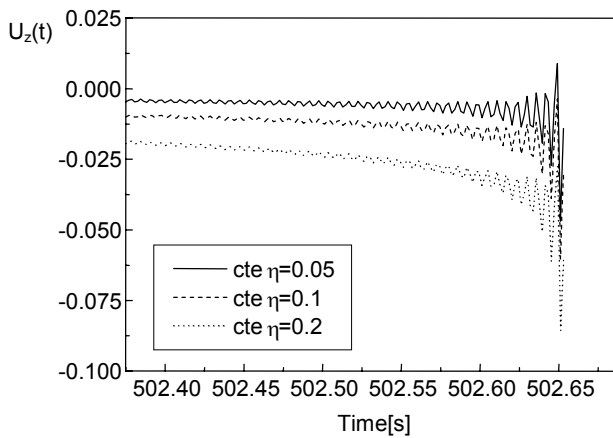


Figure 17: Analysis of causality- constant hysteretic model Figure 18: Analysis of causality- model comparison, $\eta=0.1$

5. Concluding remark

A methodology to synthesize the transient response of 2D flexible and massless foundations resting on transverse isotropic viscoelastic layer is outlined in the present paper. The method is based on response functions calculated in the frequency domain and transformed to the time domain by the FFT algorithm. The procedure is applied to investigate the effects of distinct viscoelastic soil models and parameters. The constant hysteretic, the Kelvin–Voigt and a “ramp-like” damping models are investigated. The effect of the models on the causality of the time response is also reported. The influences of the layer depth and continuum degree of anisotropy are investigated. The numerically determined transient response is correlated to the wave propagation phenomena taking place on the layer.

6. Acknowledgement

FAPESP, CAPES and FAEP have supported the research leading to the article. This is gratefully acknowledged.

7. References

- Adolph, M., 2002, Soluções Transientes de Problemas Visco-Elastodinâmicos em Meios Ilimitados através da Transformada de Fourier Rápida – FFT, M. Sc. Thesis, Faculdade de Engenharia Mecânica, Universidade de Campinas, Brasil.
- Barros, P.L.A., 1997, Elastodinâmica de Meios Transversalmente Isotrópicos: Funções de Green e o Método dos Elementos de Contorno na Análise da Interação Solo-estrutura, Ph. D. Thesis, Faculdade de Engenharia Mecânica, Universidade de Campinas, Brasil.
- Barros, P.L.A., Mesquita, E., 1999, Elastodynamic Green’s Functions for Orthotropic Plane Strain Continua with inclined Axis of Symmetry, *International Journal for Solids and Structures*, vol. 36, pp. 4767-4788.
- Beskos, D, 1987, *Boundary Element Methods in Dynamics Analysis*, *Applied Mechanics Review*, vol. 40, n. 1.
- Beskos, D, 1997, *Boundary Element Methods in Dynamics Analysis: Part II (1986-1996)*, *Applied Mechanics Review*, vol. 50, n. 3.
- Domingues, J., 1993, *Boundary Elements in Dynamics*. Computational Mechanics Publications, Southampton, UK.
- Mesquita, E., Barros, P.L.A., Pavanello, R., Adolph, M., Romanini, E., 2002, Dinâmica dos Meios Ilimitados e o Método dos Elementos de Contorno, *Anais do I Congresso de Dinâmica, Controle e Aplicações*, Editor J. M. Balthazar, M. Boaventura, G. N. Silva and M. Tsuchida, Sociedade Brasileira de Matemática Aplicada e Computacional – SBMAC, vol 1, pp 77-83.
- Richard Jr, F. E., Hall, J. R., Woods, R. D., 1970, *Vibration of Soils and Foundations*, Prentice Hall, Englewood Cliffs, New Jersey.
- Sommerfeld, A., 1949, *Partial Differential Equations*, Academic Press, New York.
- Zavala, P. A. G., Pavanello, R., 1999, Vibro-acoustic Modeling in Infinite Fluid Medium using the Finite Element Method with DTN MAP. *Anais do XV Congresso Brasileiro de Engenharia Mecânica*, Águas de Lindóia SP, Brasil, 22-26 november. 10pp (CD-ROM).